

Dust Evolution in the Dwarf Galaxy Holmberg II

D.S. Wiebe ^{1,*}, M.S. Khramtsova ¹, O.V. Egorov ², T.A. Lozinskaya ²

ABSTRACT

A detailed photometric study of star-forming regions (SFRs) in the galaxy Holmberg II has been carried out using archival observational data from the far infrared to ultraviolet obtained with the GALEX, Spitzer, and Herschel telescopes. Spectroscopic observations with the 6-m telescope of Special Astrophysical Observatory of the Russian Academy of Sciences are used to estimate ages and metallicities of SFRs. For the first time, the ages of SFRs have been related to their emission parameters in a wide spectral range and with the physical parameters determined by fitting the observed spectra. It is shown that fluxes at 8 and 24 μm characterizing the emission of polycyclic aromatic hydrocarbons (PAHs) and hot dust grains decrease with age, but their ratio increases. This implies that the relative PAH contribution to the total infrared flux increases with age. It is suggested that the detected increase in the ratio of the fluxes at 8 and 24 μm is related to the growth in the PAH mass due to destruction of larger grains.

Subject headings: interstellar medium, dust, star-forming regions.

INTRODUCTION

Despite its relatively small mass fraction ($\sim 1\%$), dust plays an important role in the evolution of galaxies both on a global scale and in individual star-forming regions (SFRs). It is also a valuable diagnostic tool, because in late-type galaxies a significant fraction of the bolometric luminosity is generated by dust grains of various types.

Among the various interstellar dust components, the so-called polycyclic aromatic hydrocarbon (PAH) macromolecules, which are presumably responsible for the formation of unidentified infrared (IR) bands (UIBs), have attracted particular attention in recent years. Their IR emission is believed to be generated by the reradiation of absorbed ultraviolet (UV) photons (Draine and Li 2007) and, therefore, can serve as a star formation rate indicator (Calzetti 2011). However, the utilization of PAHs for this purpose is hampered by the lack of necessary understanding of

their formation and destruction processes. The key problem is the twofold role of the UV radiation in the evolution of PAHs. UV photons excite IR transitions in PAH molecules but also simultaneously destroy these molecules. Therefore, the dependence of the PAH band intensity on UV radiation can be nonmonotonic.

One of the best-known properties of PAHs is the dependence of their relative abundance on metallicity. Specifically, the q_{PAH} parameter characterizing the PAH fraction in the total dust mass decreases from a few percent in solar-metallicity galaxies to a fraction of a percent in galaxies with an oxygen abundance $12 + \log(\text{O}/\text{H})$ lower than 8.1 (Draine et al. 2007; Madden et al. 2006; Hunt et al. 2010; Engelbracht et al. 2005). It was shown in several studies (Gordon et al. 2008; Wiebe et al. 2011; Khramtsova et al. 2013) that this correlation not only is observed for galaxies as a whole but is also traceable for individual SFRs inside galaxies.

A detailed study of the IR emission in individual extragalactic SFRs has become possible owing to the Spitzer and Herschel space observatories. The angular resolution of their instruments is sufficient to investigate the spatial distribution of

¹Institute of Astronomy, Russian Academy of Sciences, Pyatnitskaya ul. 48, Moscow, 109017 Russia

²Lomonosov Moscow State University, Sternberg Astronomical Institute, Universitetskii pr. 13, Moscow, 119992 Russia

*E-mail: dwiebe@inasan.ru

emission from dust grains of various types in star-forming complexes (though insufficient to investigate individual HII regions). Detailed mapping of the IR emission, the dust temperature, and the PAH mass fraction (q_{PAH}) allows relating these quantities to other *local* properties of SFRs, for example, to the intensity of their UV radiation and metallicity. However, despite the large volume of observational data, low-metallicity galaxies have not yet been adequately studied in this respect.

Based on Spitzer and Herschel observational data and published metallicity data, Khramtsova et al. (2013) investigated the relation between the oxygen abundance $12 + \log(\text{O}/\text{H})$ and the PAH mass fraction q_{PAH} in more than 200 extragalactic SFRs. These authors showed the PAH abundance in high-metallicity SFRs to increase with oxygen abundance and concluded that the PAH abundance–metallicity correlation is most likely related to their more efficient destruction in the interstellar medium with lower abundance of heavy elements. However, the data turned out to be insufficient to analyze in detail the behavior of q_{PAH} in the lowest-metallicity SFRs.

This paper presents a detailed study of the dwarf galaxy Holmberg II (Ho II). As this galaxy was included in several large surveys, for example, SINGS (Kennicutt et al. 2003), THINGS (Walter et al. 2008), HERACLES (Leroy et al. 2009), and KINGFISH (Kennicutt et al. 2011), it was thoroughly mapped in many spectral ranges, from X rays to 21 cm. Both Spitzer observational data at 8 and 24 μm and longer-wavelength Herschel data, which allow characterizing not only the PAH abundance but also the abundance of larger dust grains are available for the galaxy.

Numerous “holes” and expanding supergiant shells (SGSs) are a characteristic feature of the HI distribution in Ho II. Puche et al. (1992) isolated 51 SGSs in the galaxy with a total kinetic energy of about 10^{53} erg. A slightly smaller number of shells (39) were identified by Bagetakos et al. (2011) using the different criteria to classify a structure as a hole or a supershell; they mostly coincide with SGSs from Puche et al. (1992). The shell sizes vary between 0.26 and 2.11 kpc, corresponding to a kinematic age from 10 to 150 Myr for expansion velocities of 7–20 km s^{-1} (Bagetakos et al. 2011).

It was previously thought that the origin of a supershell is related to the combined action of stel-

lar winds and supernova explosions in a young stellar association. However, the search for parent associations in Ho II shells undertaken by Weisz et al. (2009) using detailed multicolor photometry based on Hubble Space Telescope observations was unsuccessful. More precisely, several stellar groups of different ages were found within many of the shells. Weisz et al. (2009) concluded that the giant cavities in the HI distribution were produced not by one star cluster but by several generations of stars that had been born over hundreds of millions of years.

Thus, the structure of the interstellar medium in Ho II indicates that active star formation has taken place in the galaxy over the last several hundred million years. Hodge et al. (1994) revealed 82 HII complexes in the galaxy concentrate mainly in the directions of the highest HI column density and form several chains of active SFRs, the brightest of which are located in the eastern chain. Another study of HII regions in the galaxy Ho II was undertaken by Stewart et al. (2000). These authors estimated the ages of 45 HII regions and divided them into four age groups. Most of the regions fell into the groups with an age younger than 6.3 Myr. This is consistent with other estimates of the star formation history in Ho II, according to which the star formation rate in the galaxy has increased over the last several million years (Weisz et al. 2008). This implies that we have an opportunity to study in detail the evolution of young SFRs in a low-metallicity galaxy.

Here, we investigate the dust component of Ho II and relate its properties to the ionized-gas metallicity, the ages of SFRs, and the emission parameters in them. We use GALEX, Spitzer, and Herschel archival observational data for Ho II and the observations of Ho II with the Russian 6-m telescope at the Special Astrophysical Observatory of the Russian Academy of Sciences (SAO RAS).

OBSERVATIONAL DATA

A characteristic feature of the Ho II galaxy that distinguishes it, for example, from the Small Magellanic Cloud or the IC 10 galaxy is a nearly complete absence of extended emission at 8 μm . The emission at 8 μm is assumed to be generated mainly through the fluorescence of ionized PAH molecules and, therefore, we may conclude that

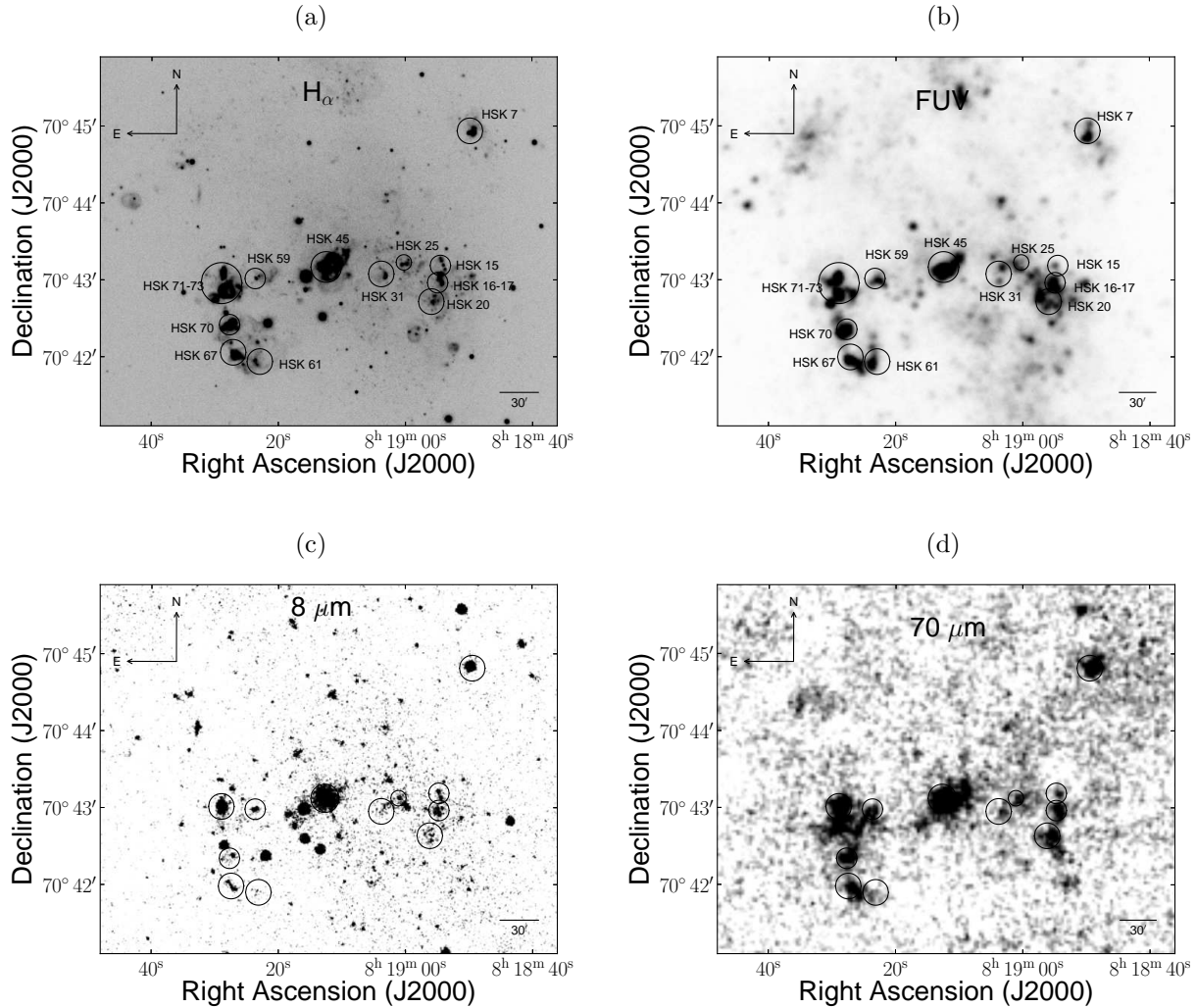


Fig. 1.— Location of studied SFRs in the Ho II galaxy identified according to Hodge et al. (1994): (a) the $H\alpha$ galaxy image from Kennicutt et al. (2003); (b) GALEX FUV image; (c), (d) $8\text{-}\mu\text{m}$ (left) and $70\text{-}\mu\text{m}$ (right) images from the Spitzer space telescope.

either the PAH molecules themselves or the UV radiation needed to excite their IR bands is mostly absent in Ho II. The first alternative seems to be more likely, as diffuse UV radiation is visible in the GALEX images of the galaxy. In addition, the galaxy is observed neither in CO emission (Leroy et al. 2009) nor in long-wavelength dust emission (Hunter et al. 1986), suggesting the absence of significant amounts of absorbing material that could shield the UV radiation.

Nevertheless, there are isolated HII complexes in Ho II that are IR emission sources. Khramtsova

et al. (2013) considered the IR emission properties in six HII complexes in the galaxy Ho II for which Moustakas et al. (2010) provided metallicities. In more detail the galaxy’s metallicity was studied by Egorov et al. (2013). As a result, in this study for our analysis we were able to select 12 complexes in active star-forming regions that are simultaneously visible in the $8\text{-}\mu\text{m}$, $24\text{-}\mu\text{m}$, and $H\alpha$ maps. Below, we use designations of HII complexes according to Hodge et al. (1994); they were all also included in the list by Stewart et al. (2000). The locations of the chosen regions are shown in Fig. 1:

(a) the H α map of the galaxy obtained with the 2.1-m KPNO telescope (Kennicutt et al. 2003), (b) the FUV map obtained with the GALEX space telescope, and (c), (d) the IR maps in the 8- and 70- μm bands.

To analyze SFRs in the Ho II galaxy, we used the spectroscopic observations performed with the 6-m SAO RAS telescope and presented in Egorov et al. (2013). We retrieved the Spitzer observations at wavelengths from 3.6 to 24 μm from the SINGS¹ archive (Kennicutt et al. 2003). Observational data at 70 and 160 μm are downloaded from the Herschel Science Archive², and the UV data are taken from the GALEX archive (in the FUV and NUV filters).

The procedures for data reduction and IR aperture photometry are described in detail in Khramtsova et al. (2013), so here we present only a brief description. The images from different instruments and at different wavelengths are characterized by different point spread functions (PSFs). To reduce all our data to a single angular resolution, we convolved them using the programs described by Aniano et al. (2011). In addition, the data were converted to common physical units (Jy/pixel). The obtained images were used for aperture photometry in all available filters. The aperture radii were chosen in such a way that the SFR entirely fell within the aperture at all wavelengths. We did not use apertures smaller than 12'', which is the minimum angular resolution. Since a typical SFR occupies no more than a few pixels (especially at 160 μm), the contribution from incomplete pixels was taken into account in the total flux. The background emission was subtracted for each pixel within the aperture. A linear interpolation of the flux in the surrounding pixels or, more precisely, in a ring with a width of several arcsec was applied in the calculation.

To estimate the dust parameters, we used the model of Draine and Li (2007). In this model the dust IR spectrum is computed under assumption that the radiation field in the investigated SFR is described by the expression

$$u_\nu = U u_\nu^{\text{MMP83}},$$

¹<http://sings.stsci.edu>

²http://herschel.esac.esa.int/Science_Archive.shtml

where U is the relative radiation intensity and u_ν^{MMP83} is the radiation field (the mean intensity or energy density) in the solar neighborhood determined by Mathis et al. (1983). It is also assumed in the model that the mass of the dust M_{dust} heated by a radiation field in the range from U_{min} to U_{max} can be estimated from the distribution

$$\frac{dM_{\text{dust}}}{dU} = (1 - \gamma)M_{\text{dust}}\delta(U - U_{\text{min}}) + \gamma M_{\text{dust}} \frac{\alpha - 1}{U_{\text{min}}^{1-\alpha} - U_{\text{max}}^{1-\alpha}} U^{-\alpha}.$$

Here, U_{min} is the minimum (background) radiation field in the investigated object, U_{max} is the maximum radiation field, and δ is the delta function. It was shown by Draine et al. (2007) that results of calculations are only weakly dependent on U_{max} and exponent α , so they can be fixed to reduce the number of free parameters. Based on observational data for the Milky Way, Draine et al. (2007) proposed values of 10^6 and 2, respectively, for these parameters. The mass fraction of dust illuminated by an enhanced radiation field (greater than U_{min}) is γ . The dust is assumed to be described by the size distribution from Weingartner and Draine (2001) with a PAH mass fraction q_{PAH} .

Using the least-squares method, for each SFR we found the model that best fits the observations at 3.6, 4.5, 5.8, 8.0, 24, 70, 100, and 160 μm , determining the following parameters of the SFR: the PAH mass fraction q_{PAH} , the minimum intensity of the dust-heating radiation field, the fraction of the dust heated by an enhanced radiation field, and the dust mass. The observations at 3.6 μm were used to subtract the stellar background by the technique described in Marble et al. (2010). The Monte Carlo method was used to determine the parameter estimation errors.

Using on our aperture photometry, we calculated the following flux ratios:

$$P_8 = \frac{\nu F_\nu^{\text{NS}}(8 \mu\text{m})}{\nu F_\nu(70 \mu\text{m}) + \nu F_\nu(160 \mu\text{m})},$$

$$P_{24} = \frac{\nu F_\nu^{\text{NS}}(24 \mu\text{m})}{\nu F_\nu(70 \mu\text{m}) + \nu F_\nu(160 \mu\text{m})},$$

$$R_{71} = \frac{\nu F_\nu(70 \mu\text{m})}{\nu F_\nu(160 \mu\text{m})}.$$

Here, ν denotes the central frequency of the filter. The superscript “ns” denotes the flux from which the stellar contribution was subtracted. This component was subtracted from the fluxes at 8 and 24 μm . The results of the UV photometry are presented as FUV and NUV magnitudes. Apart from the metallicities, emission line intensities were also taken from Egorov et al. (2013). The results of the photometry are presented in Table 1.

THE AGES OF STAR-FORMING REGIONS

As was shown by Copetti et al. (1986), the equivalent width of the $\text{H}\beta$ emission line correlates well with an age of an HII region, while being virtually independent of the electron temperature of the medium. This correlation arises because the number of ionizing photons from massive stars decreases with age, while the continuum level from low-mass stars at $\text{H}\beta$ wavelength increases. The possibility of using $\text{EW}(\text{H}\beta)$ as an age indicator was demonstrated in several studies (see, e.g., Schaerer and Vacca 1998; Leitherer et al. 1999).

In this paper, to estimate ages we use the grid of models presented by Levesque et al. (2010) based on the evolutionary tracks from Schaerer and Vacca (1998) for various metallicities. However, this method has several shortcomings described in detail by Stasińska and Leitherer (1996), with the main one being the assumption about a single stellar population in a given HII complex. If there are stars of previous generations in the HII complex, then they can raise the continuum level, thereby reducing the $\text{H}\beta$ equivalent width and, accordingly, overestimating the age. In addition, internal extinction in the HII complex can decrease the number of ionizing photons. However, the dust mass in Ho II is insignificant and extinction should not affect our results significantly.

To assess the correctness of the SFR age estimates, we used observations of Ho II performed at the 6-m SAO RAS telescope with a Fabry–Perot interferometer (FPI) in $\text{H}\alpha$ and $[\text{SII}]$ 6717 \AA lines. (A detailed study of the ionized and neutral gas kinematics in the galaxy will be presented in the paper by Egorov, Lozinskaya, and Moiseev being prepared for publication.) The derived data cubes were used to estimate the expansion velocities of SFRs and to determine their kinematic

Table 2: Comparison between ages determined from the $\text{H}\beta$ equivalent width and kinematic ages

Region	V_{exp} , km s^{-1}	Diameter, arcsec	Age, Myr	Age ($\text{H}\beta$), Myr
HSK15	< 9	2.8	> 1.5	4.8
HSK16–17	< 9(6)	6.9	> 2.3(5.6)	5.3
HSK20	< 9	4.0	> 2.2	5.3
HSK25	< 9	4.6	> 2.5	6.2
HSK31	< 9(4)	6.2	> 3.4(7.6)	6.3
HSK45	16	11.3	> 3.5	3.7
HSK59	< 9(4)	2.0	> 1.1(2.5)	4.1
HSK61	< 9(5)	3.8	> 2.1(3.7)	7.7
HSK67	< 9(6)	4.3	> 2.4(3.5)	3.8
HSK70	< 9(6)	6.3	> 3.4(5.2)	4.8
HSK71	< 9	4.7	> 2.6	3.5
HSK73	10	7.5	> 3.7	3.5

ages. We attempted to determine the expansion velocity from the characteristic splitting of the position–velocity (PV) diagrams for shell-like HII complexes, but no such evidence was revealed in most of the discussed regions. Their expansion is only revealed by the increasing line FWHM toward the center of the region. To estimate the expansion velocity roughly, in each complex we identified locations of the radial velocity minimum and maximum and assumed that the minimum and maximum velocities correspond to the emission from bright parts of the approaching and receding sides of the shell, respectively. The results are presented in Table 2. For regions where the inferred expansion velocity turned out to be smaller than the FPI resolution (18 km s^{-1}), in Table 2 we give an upper limit for the expansion velocity equal to 9 km s^{-1} , while the value formally found from our data is given in parentheses. The value of 9 km s^{-1} was also assumed in cases where we failed to obtain an estimate of the expansion velocity. Typical uncertainty of expansion velocity measurements is 2 km s^{-1} .

The kinematic age was estimated from the model of Mac Low and McCray (1988). For an expanding supershell driven by the combined action of supernovae and stellar winds, we used the relation

$$t \approx 0.6R/V_{\text{exp}},$$

where R is the radius in parsecs, V_{exp} is the expansion velocity in km s^{-1} , and t is the age in Myr. As can be seen from Table 2, we were able to estimate

Table 1: Results of the photometry for SFRs in the Holmberg II galaxy (the numbers in parentheses indicate powers of 10)

Region	F_8	F_{24}	F_{70}	F_{100}	F_{160}	FUV	NUV
HSK7	$6.6(-4) \pm 2.2(-3)$	$8.7(-3) \pm 1.9(-4)$	$6.9(-2) \pm 2.7(-3)$	$6.8(-2) \pm 3.9(-3)$	$3.7(-2) \pm 1.9(-3)$	16.85 ± 0.08	16.81 ± 0.04
HSK15	$6.9(-5) \pm 1.3(-5)$	$6.7(-4) \pm 8.5(-5)$	$5.9(-3) \pm 2.2(-3)$	$8.6(-3) \pm 2.6(-3)$	$3.7(-3) \pm 2.4(-3)$	19.93 ± 0.33	20.14 ± 0.36
HSK16-17	$1.2(-4) \pm 8.9(-6)$	$1.1(-3) \pm 6.0(-5)$	$1.7(-2) \pm 1.9(-3)$	$2.2(-2) \pm 1.8(-3)$	$1.3(-2) \pm 1.5(-3)$	17.37 ± 0.11	17.45 ± 0.11
HSK20	$9.4(-5) \pm 1.0(-5)$	$8.1(-4) \pm 6.1(-5)$	$2.6(-2) \pm 3.2(-3)$	$3.1(-2) \pm 3.7(-3)$	$1.8(-2) \pm 3.0(-3)$	17.48 ± 0.27	17.42 ± 0.25
HSK25	$2.2(-4) \pm 1.4(-5)$	$7.1(-4) \pm 8.2(-5)$	$1.3(-2) \pm 1.4(-3)$	$2.2(-2) \pm 3.6(-3)$	$2.2(-2) \pm 3.8(-3)$	19.38 ± 0.42	19.24 ± 0.37
HSK31	$8.6(-5) \pm 2.1(-5)$	$4.1(-4) \pm 6.5(-5)$	$7.0(-3) \pm 2.2(-3)$	$1.2(-2) \pm 2.6(-3)$	$1.3(-2) \pm 2.7(-3)$	19.34 ± 0.20	19.64 ± 0.26
HSK45	$6.1(-3) \pm 3.1(-4)$	$2.1(-2) \pm 3.2(-4)$	$1.1(-1) \pm 6.4(-3)$	$1.2(-1) \pm 7.1(-3)$	$6.9(-2) \pm 4.5(-3)$	15.06 ± 0.02	15.33 ± 0.05
HSK59	$8.0(-5) \pm 1.1(-5)$	$1.2(-3) \pm 1.3(-4)$	$7.1(-3) \pm 3.2(-3)$	$6.3(-3) \pm 3.0(-3)$	$5.3(-3) \pm 2.0(-3)$	18.13 ± 0.06	18.19 ± 0.10
HSK61	$2.8(-5) \pm 9.3(-6)$	$2.0(-4) \pm 8.5(-5)$	$1.2(-2) \pm 3.6(-3)$	$2.1(-2) \pm 4.0(-3)$	$1.4(-2) \pm 2.7(-3)$	18.07 ± 0.15	18.06 ± 0.14
HSK67	$1.3(-3) \pm 1.1(-4)$	$2.1(-3) \pm 1.8(-4)$	$2.7(-2) \pm 2.4(-3)$	$2.3(-2) \pm 2.9(-3)$	$1.5(-2) \pm 1.2(-3)$	17.28 ± 0.14	17.43 ± 0.14
HSK70	$1.2(-3) \pm 3.9(-5)$	$1.1(-3) \pm 7.9(-5)$	$1.5(-2) \pm 1.8(-3)$	$1.7(-2) \pm 2.8(-3)$	$7.0(-3) \pm 1.7(-3)$	15.74 ± 0.04	15.89 ± 0.06
HSK71-73	$1.2(-2) \pm 2.7(-4)$	$2.2(-2) \pm 4.4(-4)$	$7.7(-2) \pm 6.5(-3)$	$6.6(-2) \pm 6.6(-3)$	$3.1(-2) \pm 3.7(-3)$	16.50 ± 0.14	16.54 ± 0.13

Table 3: Model parameters of SFRs in the Holmberg II galaxy

Region	$12 + \log(\text{O}/\text{H})$	$q_{\text{PAH}}, \%$	U_{min}	γ	$M_{\text{dust}}, M_{\odot}$	Age, Myr	Age group (Stewart et al. 2000)	F_8/F_{24}	$[\text{OIII}]/\text{H}\beta$
HSK7	7.76 ± 0.03	0.41 ± 0.04	23.51 ± 0.87	$6.6(-2) \pm 1.1(-2)$	31.8 ± 15.2	3.7 ± 0.1	0-3.5	0.050 ± 0.002	4.3 ± 0.2
HSK15	7.63 ± 0.10	0.48 ± 0.01	17.99 ± 3.35	$4.2(-2) \pm 1.2(-2)$	4.1 ± 0.7	4.8 ± 0.1	3.5-4.5	0.021 ± 0.023	1.6 ± 0.1
HSK16-17	7.68 ± 0.05	0.48 ± 0.04	13.56 ± 0.55	$2.0(-2) \pm 8.0(-3)$	16.0 ± 2.2	5.3 ± 0.2	3.5-4.5	0.062 ± 0.010	2.1 ± 0.1
HSK20	7.45 ± 0.04	0.45 ± 0.07	20.57 ± 0.29	$3.0(-3) \pm 2.0(-3)$	16.8 ± 8.6	5.3 ± 0.2	4.5-6.3	0.079 ± 0.016	1.0 ± 0.1
HSK25	7.53 ± 0.02	1.12 ± 0.52	2.76 ± 0.14	$1.5(-2) \pm 7.0(-3)$	73.8 ± 36.6	6.2 ± 0.2	4.5-6.3	0.181 ± 0.032	1.1 ± 0.02
HSK31	7.97 ± 0.12	0.91 ± 0.04	2.09 ± 0.35	$1.6(-2) \pm 6.0(-3)$	53.4 ± 17.6	6.3 ± 0.2	4.5-6.3	0.149 ± 0.058	3.3 ± 0.04
HSK45	7.89 ± 0.03	2.95 ± 0.22	16.49 ± 1.90	$1.1(-1) \pm 4.4(-2)$	75.9 ± 16.6	3.7 ± 0.1	0-3.5	0.199 ± 0.009	3.6 ± 0.02
HSK59	7.60 ± 0.03	0.56 ± 0.13	6.84 ± 1.41	$1.1(-1) \pm 5.1(-2)$	8.0 ± 4.7	4.1 ± 0.1	3.5-4.5	0.059 ± 0.012	1.8 ± 0.02
HSK61	7.66 ± 0.03	0.50 ± 0.04	3.06 ± 0.64	$1.0(-4) \pm 9.9(-5)$	51.6 ± 6.2	7.7 ± 0.2	3.5-4.5	0.084 ± 0.070	2.1 ± 0.03
HSK67	7.57 ± 0.01	0.40 ± 0.12	10.46 ± 1.46	$4.5(-2) \pm 8.0(-3)$	24.4 ± 7.0	3.8 ± 0.1	0-3.5	0.035 ± 0.006	3.0 ± 0.02
HSK70	7.72 ± 0.01	0.44 ± 0.10	25.00 ± 1.28	$2.9(-2) \pm 7.0(-3)$	7.3 ± 2.9	4.8 ± 0.1	3.5-4.5	0.037 ± 0.066	2.9 ± 0.02
HSK71-73	7.72 ± 0.04	0.48 ± 0.12	25.00 ± 1.59	$2.3(-1) \pm 3.8(-2)$	23.3 ± 5.4	3.5 ± 0.1	0-3.5	0.038 ± 0.001	2.2 ± 0.02

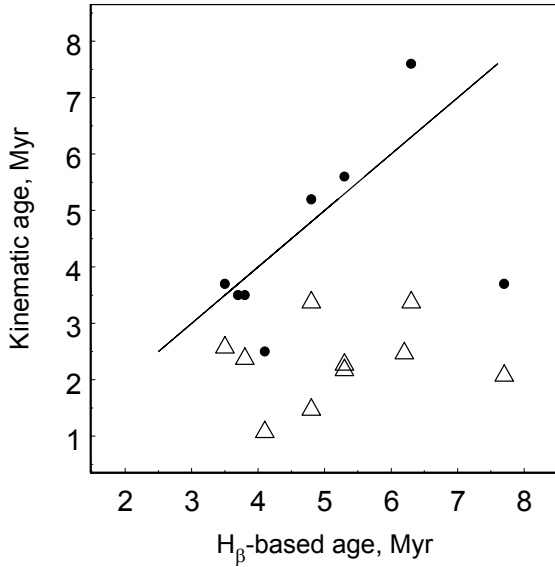


Fig. 2.— Comparison of ages determined from the $\text{H}\beta$ equivalent width and the kinematic ages of SFRs. The black circles and triangles indicate formal kinematic age estimates and lower age limits, respectively. The straight line corresponds to the equality of the two age estimates.

reliably the kinematic age only in two considered regions, HSK45 and HSK73. For a few more regions, we obtained rough estimates.

Overall, given the mentioned errors in the kinematic age estimates and the model dependence of the estimates based on the $\text{H}\beta$ equivalent width, Fig. 2 shows an agreement between the results obtained with the two methods. The only exception is the HSK61 region in which the $\text{H}\beta$ line has the smallest equivalent width corresponding to an age of more than 7 Myr constitutes.

RESULTS

The results of fitting the spectra of 12 investigated SFRs are shown in Fig. 3, and the corresponding parameters of the dust emission models are presented in Table 3. As can be seen from Fig. 3, the grid of models from Draine and Li (2007) is insufficient to fit the spectra at a low PAH band intensity, in particular at $8 \mu\text{m}$. Therefore, for almost all of the SFRs, with the exception of HSK25, HSK31, and HSK45, values of q_{PAH} are upper limits. Below, we will use the ratio of fluxes at 8 and $24 \mu\text{m}$, F_8/F_{24} , as a PAH abundance indicator. Sandstrom et al. (2010) and Khramtsova et al. (2013) showed that when individual SFRs are investigated, this ratio correlates

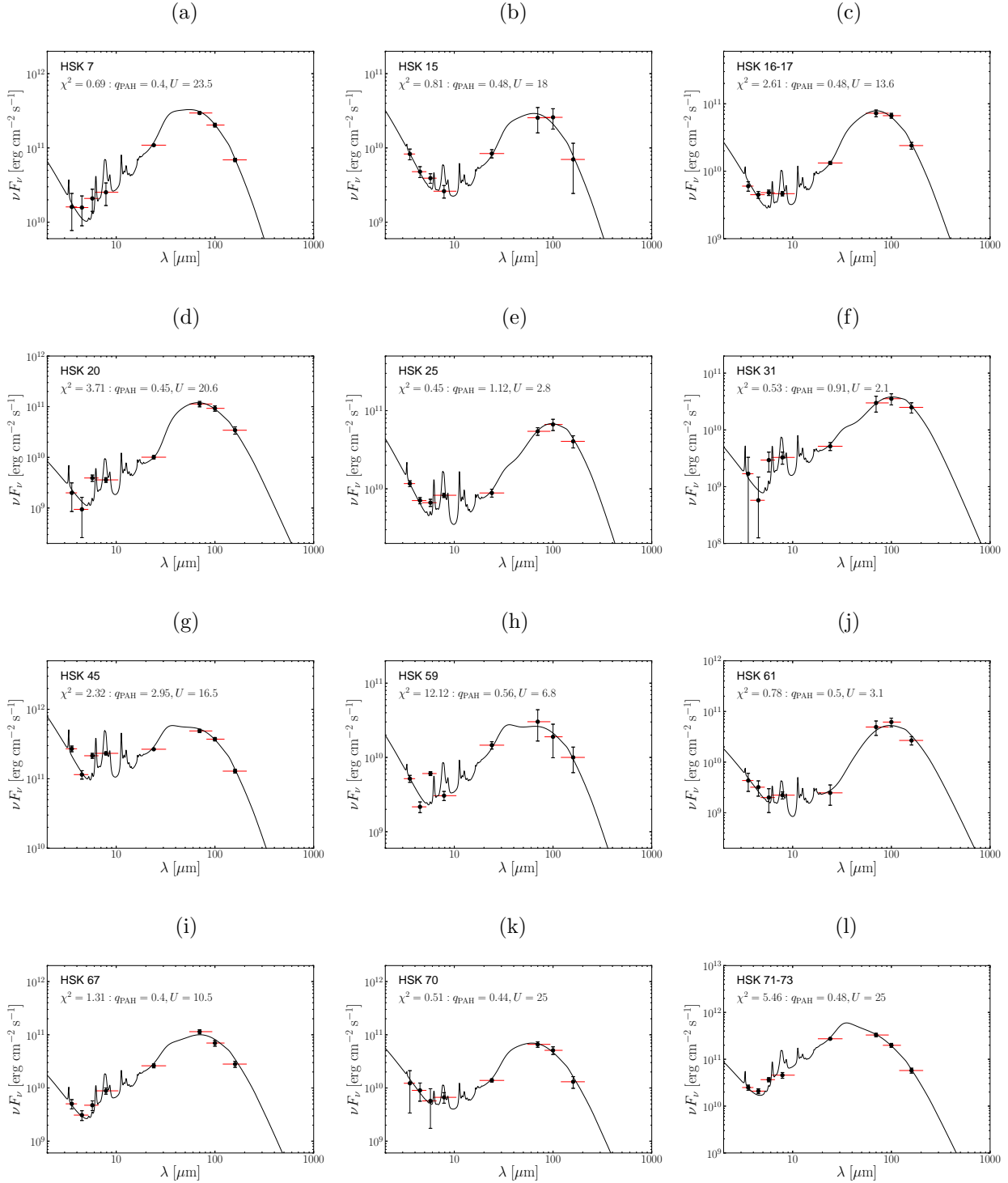


Fig. 3.— Results of fitting the spectra of SFRs in Ho II.

with q_{PAH} , albeit with some scatter. Also, we will consider the P_8 and P_{24} indices that are the ratios of fluxes in short-wavelength infrared bands to the cold dust flux. These indices were introduced by Draine and Li (2007) as near-IR emission characteristics normalized to the total dust mass by assuming it to be proportional to the sum of fluxes in long-wavelength bands (at 70 and 160 μm).

The brightest emission source at 8 μm in the Ho II galaxy is HSK45, a cavity surrounded by an $\text{H}\alpha$ emission ring. It is tempting to assume that the emission peak at 8 μm is associated with the brightest part of the ring, but a detailed comparison of the emission map at 8 μm with the $\text{H}\alpha$ emission map obtained with the Hubble Space Telescope shows that the peak at 8 μm does not coincide with the ring and may be an isolated compact background source. Since the origin of the emission at 8 μm is unclear in this case, we excluded HSK45 from the further analysis.

Khramtsova et al. (2013) pointed out that if the PAH abundance is related to metallicity-dependent photodestruction, then it should depend not only on the chemical composition but also on time. If SFRs are considered in a relatively narrow range of metallicities, the PAH abundance–metallicity correlation can be blurred by evolutionary effects. This is actually the case in Ho II. In Fig. 4, the flux ratio F_8/F_{24} and the P_8 index are plotted vs the SFR oxygen abundance; obviously, there is no correlation of both parameters with the metallicity.

To show how the parameters characterizing q_{PAH} change with time, in Figs. 5a–5c we plot the F_8/F_{24} flux ratio, the P_8 index, and the P_{24} index against the SFR age. As can be seen from the figure, F_8/F_{24} , which is numerically equal to P_8/P_{24} , increases with age, reflecting the growing (with time) relative contribution of particles emitting at 8 μm . At the same time, both P_8 and P_{24} indices decrease with SFR age.

As has been pointed out above, the P_8 and P_{24} indices were introduced under the assumption that the sum of the fluxes in long-wavelength bands (at 70 and 160 μm) characterizes the total dust content. In our data, however, the R_{71} index characterizing the radiation field intensity depends on age (Fig. 5d), suggesting that the flux not only at 8 and 24 μm but also in longer-wavelength bands changes with time and, hence, cannot be an un-

ambiguous indicator of the dust mass. Out of the bands we consider, the flux at 160 μm is least dependent on age. Figures 5e and 5f show the ratios of the fluxes at 8 and 24 μm to the flux at 160 μm . Since the emission at 160 μm is relatively constant in the considered time interval, these ratios hopefully reflect the evolution of the fluxes at 8 and 24 μm more adequately. They point to a gradual weakening of the near-IR emission as well.

Two effects can be responsible for the decreasing intensity of radiation from PAH particles and very small grains: the destruction of emitting particles and the reduction in the intensity of UV radiation heating very small grains and exciting vibrations and bending in PAH macromolecules. The heated big grains, for which significant destruction is not expected, must be the main source of emission at wavelengths longer than ~ 30 μm . Therefore, only weakening radiation can be responsible for the gradual decrease of the R_{71} index. In the model of Draine and Li (2007), the grain-heating radiation field is characterized by several parameters, out of which we consider the minimum SFR radiation field, U_{min} , and the grain mass fraction γ affected by a radiation field with intensity exceeding U_{min} . These two parameters are plotted against time in Figs. 6a and 6b.

Both parameters decrease with time, which seems natural: as the SFR evolves, the minimum radiation field should weaken after the initial starburst, while the fraction of dust affected by an enhanced radiation field should decrease. The correlation of U_{min} with age is noticeably weaker than the correlation of γ with age. This is probably because γ depends more strongly on the number of most massive and short-lived stars. Figures 6c and 6d show the radiation hardness parameters, the FUV–NUV magnitude difference and the $[\text{OIII}]\lambda 5007 \text{ \AA}/\text{H}\beta$ line ratio, for SFRs of various ages. As can be seen, the correlation is either weak or absent in both cases.

Figure 7a shows how the dust mass correlates with U_{min} in the investigated SFRs. All SFRs on this diagram can be arbitrarily divided into two groups: with a lower mass and a stronger radiation field and with a higher mass and a weaker radiation field. The second group includes HSK25, HSK31, and HSK61 for which the emission peaks at about 100 μm (see Fig. 3). For the remaining regions, the peak occurs at shorter wavelengths, cor-

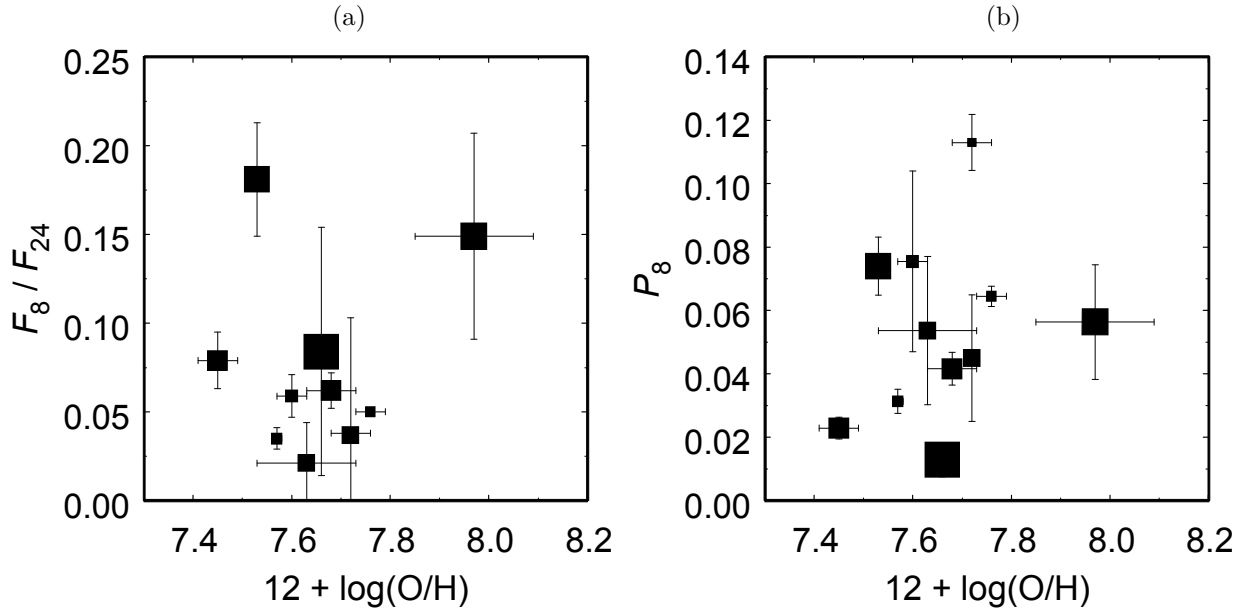


Fig. 4.— Flux ratio F_8/F_{24} (a) and P_8 index (b) versus metallicity. The symbol size corresponds to the SFR age from 3.5 to 7.7 Myr.

responding to a higher average dust temperature. Within the used model, this implies higher dust-heating radiation intensities. In HSK25, HSK31, and HSK61, the dust is colder than that in other regions, but their IR flux is comparable to that from some of the regions with “warm” dust. The assumption about a higher dust mass is required for its description.

However, as has been shown above, U_{\min} correlates with the age. Formally, this implies that the dust mass also correlates with the age in our data (Fig. 7b). Both real factors and observational selection can be responsible for this correlation. The absence of old low-mass regions in our list is quite expectable: in our study we selected the SFRs based on the brightness of emission at $8 \mu\text{m}$, which is too weak to be detected in old low-mass regions.

Two main factors can be responsible for the absence of young regions with a high dust mass. First, they can actually be absent due to some peculiarities of the current star formation episode, for example, because new starbursts were triggered by the stimulating action of older regions. Since the “new” regions are formed from the remaining matter, they may have a smaller scale.

However, this suggestion is speculative and requires a serious study.

Second, it can also be hypothesized that this correlation is real, for example, due to the synthesis of dust in evolved stars inside SFRs. However, the age of the regions under consideration is too small for the ejection of dust-enriched matter by asymptotic giant branch stars to have already begun in them. At present, core-collapse supernovae are also considered as an important source of dust (see, e.g., Sugerman et al. 2006; Gomez et al. 2012). In principle, an age of several million years is sufficient for the evolution of the most massive stars to have ended. However, there are no clear evidences for supernova explosions in the kinematics of SFRs.

DISCUSSION

The Ho II galaxy is a promising object for investigating the PAH life cycle in metal-poor systems. In this galaxy the emission at $8 \mu\text{m}$ (attributed to PAHs) is concentrated only in several regions coincident with HII complexes. Our spectroscopic observations and aperture photometry from archival IR and UV data allow considering possible corre-

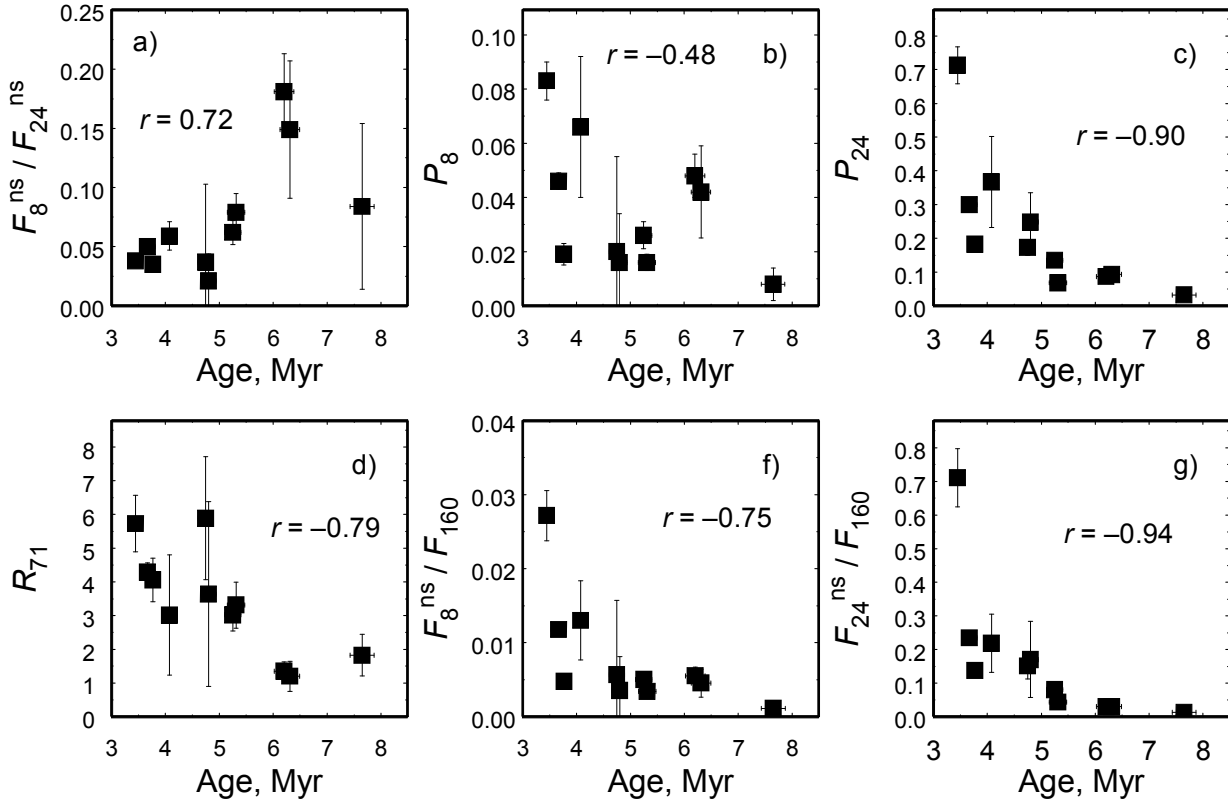


Fig. 5.— Photometric characteristics of SFRs versus age. The Spearman rank correlation coefficients are indicated.

lations between the PAH emission and other parameters of the investigated regions.

Here, we revealed the following correlations that are important for understanding the PAH life cycle in HII regions:

- the P_8 , P_{24} , and R_{71} indices characterizing the fractions of “hot” and “warm” dust as well as the field intensity decrease with time;
- the flux ratio F_8/F_{24} increases with time;
- the minimum radiation field and the fraction of dust heated by an enhanced radiation field decrease with time;
- the radiation field hardness parameters are virtually independent of time.

The absence of correlation between metallicity and PAH abundance in HII complexes of the

Ho II galaxy implies that in this case we have an opportunity to study age effects in a pure form. If the ratio F_8/F_{24} is considered as a measure of the relative PAH abundance (as was proposed in several papers; see, e.g., Sandstrom et al. 2010; Khramtsova et al. 2013), then we may conclude that the relative PAH abundance increases with time (Fig. 5a). Let us consider this conclusion in more detail.

The emission in almost all of the considered IR bands weakens with time, but, obviously, emission at $8 \mu\text{m}$ goes down more slowly than emission at $24 \mu\text{m}$. To unravel the reason, we calculated several spectra of SFRs with a dust mass $M_{\text{dust}} = 100 M_{\odot}$ and $q_{\text{PAH}} = 0.45\%$ for various γ at fixed U_{min} and for various U_{min} at fixed γ using the model of Draine and Li (2007). Results of our calculations are presented in Fig. 8 as flux ratios. Figure 8a also shows the parameters of SFRs in the galaxy Ho II estimated in this

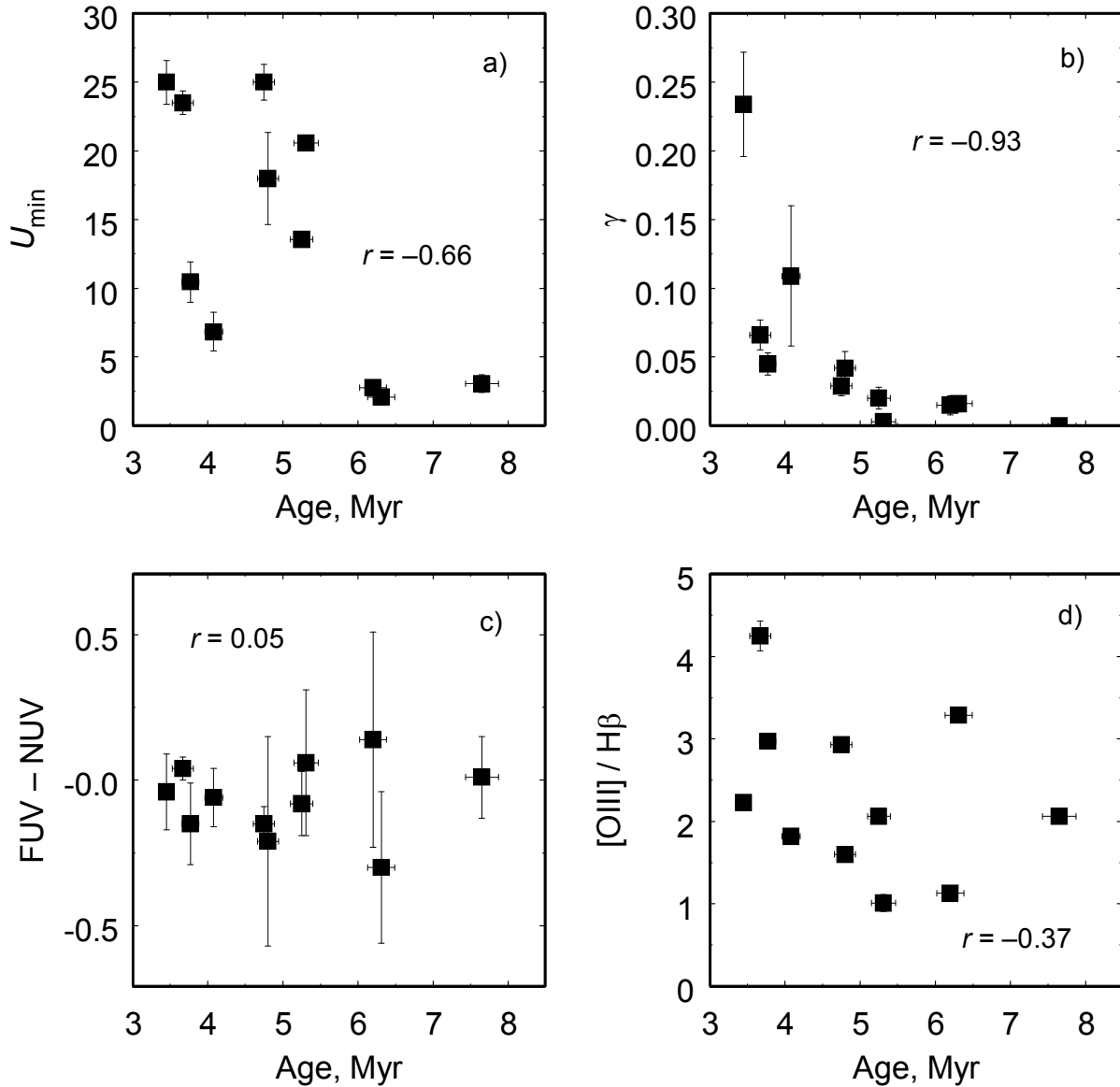


Fig. 6.— Radiation field parameters versus age: (a) minimum radiation field U_{\min} , (b) parameter γ , (c) FUV–NUV magnitude difference, and (d) $[OIII]\lambda 5007/H\beta$ line ratio. The Spearman rank correlation coefficients are indicated.

study.

The ratios of fluxes at 8 and 24 μm to the flux at 160 μm increase with γ (Fig. 8a, the dotted and dash–dotted lines), but F_8/F_{160} depends on γ not so strongly as F_{24}/F_{160} . This result is expectable, because the parameter γ in the Draine and Li (2007) model is mostly sensitive to the

flux at 24 μm . It shows the fraction of hot dust heated by a radiation field whose intensity exceeds the mean background field U_{\min} , and this field is most likely associated with the vicinities of massive stars, where the dust emission at 24 μm should be particularly strong. The fewer such regions, the weaker emission at 24 μm is observed.

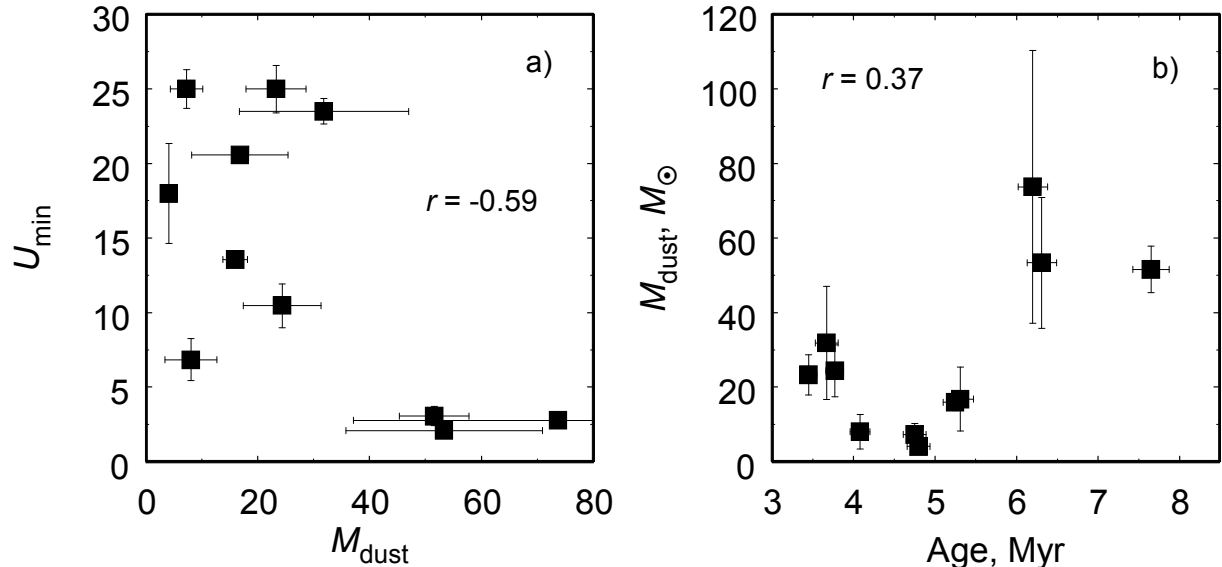


Fig. 7.— Correlation between the dust mass, the minimum radiation field, and the age. The Spearman rank correlation coefficients are indicated.

The ratio F_8/F_{24} (solid line) in the model of Draine and Li (2007) *decreases* with increasing γ , i.e., with increasing fraction of hot dust. However, this decrease is insignificant compared to the observed effect. It should be noted that the observed points fall nicely on the curves for the ratios F_8/F_{160} and F_{24}/F_{160} , but this coincidence only suggests that γ that provides the best agreement between the theoretical and observed spectra in the used model is mainly influenced by the ratio of the fluxes at short- and long-wavelengths and depends more weakly on other parameters.

In Fig. 8b, the flux ratios are plotted against the parameter U_{\min} . The same picture is observed here: as the radiation field intensity in SFRs increases, the calculated flux ratios F_8/F_{160} and F_{24}/F_{160} increase, while the ratio F_8/F_{24} decreases, but the decrease in F_8/F_{24} with increasing U_{\min} is also insignificant compared to the observed effect in this case.

These estimates show that the ratio F_8/F_{24} in “old” SFRs that is larger by several times than that in “young” SFRs only to a small extent can be attributed to the evolution of emission parameters (U_{\min} and γ), in particular, to UV field weakening.

Another factor potentially able to affect the ratio F_8/F_{24} is the destruction of macromolecules and larger grains. The emission at $24\ \mu\text{m}$ is often associated with stochastically heated very small grains (VSGs). The more rapid decrease of their emission relative to the PAH emission may imply that VSGs are less stable to the destruction by UV radiation. In addition, their destruction can itself be a PAH source (if VSGs are PAH clusters), partially compensating for the destruction of the macromolecules themselves.

In Fig. 8c, the F_8/F_{24} ratio is plotted against F_{24}/F_{160} (which correlates well with age in our sample; see Fig. 5f) for various q_{PAH} . The model of Draine and Li (2007) does not allow calculating the emission parameters for $q_{\text{PAH}} < 0.45\%$, but nearly all the observed points lie below the curve for this limiting value, approximately where the line for $q_{\text{PAH}} \sim 0.1\%$ should have run. Exceptions are HSK25 and HSK31, two of the three regions with an age of more than 6 Myr and the only two regions (apart from HSK45) for which q_{PAH} is $\sim 1\%$, i.e., definitely above the limiting value of the model. It is this picture that might be expected, if q_{PAH} is initially $\sim 0.1\%$ in young SFRs of Ho II, but then, several million years later, increases to 1% due to the less efficient destruction

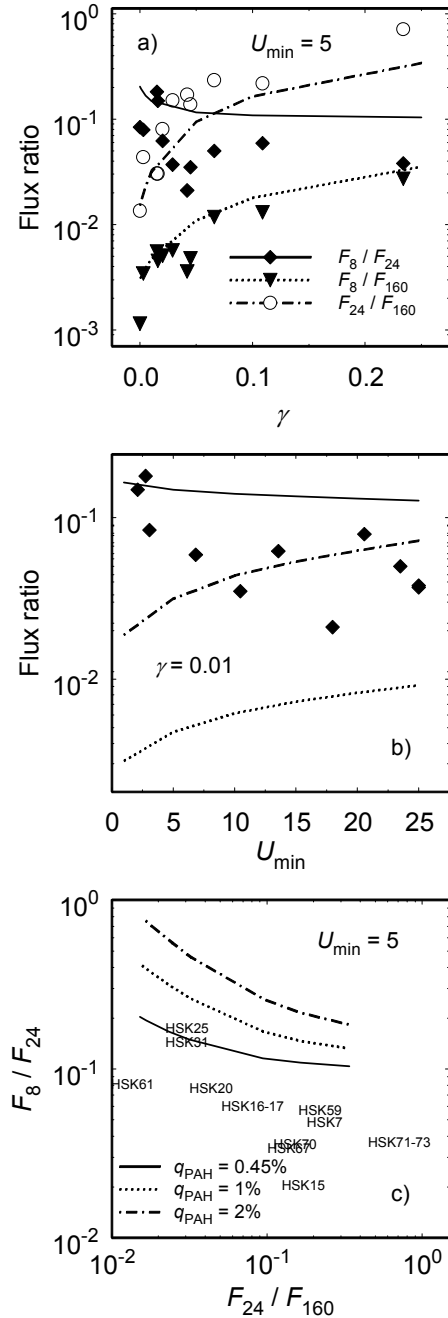


Fig. 8.— IR flux ratio versus parameters γ and U_{\min} calculated using the model of Draine and Li (2007).

of PAHs and (or) some increase in their abundance due to VSG destruction. Thus, the ratio F_8/F_{24}

and, consequently, the PAH abundance can be affected by evolutionary effects. The scatter in the correlation between F_8/F_{24} and metallicity may be related to the age differences.

As has been pointed out above, the regions that have not only an old age but also the highest mass in our sample are characterized by a relatively high PAH abundance and a less intense radiation field. The increase in the IR flux in these regions may be associated not so much with the pure evolution as with the differences in the evolution of more massive and less massive complexes, leading to different PAH abundances. In other words, not only the age of the complex but also its mass can be a factor affecting the PAH abundance. However, a sample of objects that is large enough to reveal correlations is needed to test this assumption.

HSK61, the oldest region in our sample, i.e., the region with the smallest $H\beta$ equivalent width, stands apart of the overall picture. The smallest ratio F_{24}/F_{160} in this region agrees with the old estimated age. On the other hand, this is the only region whose “spectral” age exceeds considerably the kinematic age and is well beyond the age range determined for this region by Stewart et al. (2000). Unfortunately, the available data are insufficient to determine why HSK61 differs from other SFRs in Ho II.

What is said above is valid, provided the emission at $24 \mu\text{m}$ is generated by very small grains, but this interpretation is not universally accepted. Larger grains heated to high temperatures in the vicinity of massive stars can also be a source of this emission. Such grains are probably destroyed much more slowly than PAHs and VSGs and the increase in F_8/F_{24} is more difficult to explain by their destruction. An emission generation model that, in contrast to the model of Draine and Li (2007), would allow using an arbitrary grain size distribution is needed to investigate this alternative. In conclusion, it should be noted that our conclusions are based on the application of the model by Draine and Li (2007). At present, this model is the basic one for determining the dust and field parameters from IR data, but the wide application of the model does not guarantee its universality. It may well be that the model requires a refinement. For example, the radiation field in HII complexes can differ from that specified in the model. The PAH ionization state de-

termining the intensity of the band at $8\ \mu\text{m}$ can also be different. We plan to investigate these uncertainties in a subsequent study.

CONCLUSIONS

Analyzing the archival IR, UV, and optical observational data for HII complexes in the dwarf irregular galaxy Holmberg II, we obtained the following results:

- The flux ratio F_8/F_{24} can be affected by evolutionary effects related to the destruction and formation of dust: the ratio increases as the region evolves.
- The emission at 8 and $24\ \mu\text{m}$ gets weaker with time relative to the long-wavelength emission and goes down with decreasing mean field intensity and enhanced-field fraction. The emission at $24\ \mu\text{m}$ decreases faster than that at $8\ \mu\text{m}$.
- The PAH abundance is higher in old massive complexes with a reduced radiation field.

Thus, our study shows that the fluxes at 8 and $24\ \mu\text{m}$ characterizing the emissions from PAHs and hot grains, respectively, decrease with SFR age, but their ratio increases. This implies that the relative contribution from PAHs to the total IR flux increases with age. The detected increase in the ratio of the fluxes at 8 and $24\ \mu\text{m}$ is probably related to the increase in the relative PAH fraction due to the destruction of larger grains. It should be noted that the problem being discussed is complex and requires further comprehensive studies in various wavelength ranges based on observations of a larger sample of SFRs with different ages in nearby galaxies.

ACKNOWLEDGMENTS

This work is based in part on the observational data from the BTA (SAO RAS) telescope and those taken from the archives of the Spitzer, Herschel, and GALEX space telescopes. This study was financially supported by the Russian Foundation for Basic Research (project nos. 12-02-31356 mol.a, 12-02-31452 mol.a and 14-02-00604).

REFERENCES

1. G. Aniano, B. T. Draine, K. D. Gordon, and K. Sandstrom, *Publ. Astron. Soc. Pacif.* **123**, 1218 (2011)
2. I. Bagetakos, E. Brinks, F. Walter, et al., *Astron. J.* **141**, 23 (2011).
3. D. Calzetti, *EAS Publ. Ser.* **46**, 133 (2011).
4. M. V. F. Copetti, M. G. Pastoriza, and H. A. Dottori, *Astron. Astrophys.* **156**, 111 (1986).
5. B. T. Draine and A. Li, *Astrophys. J.* **657**, 810 (2007).
6. B. T. Draine, D. A. Dale, G. Bendo, K. D. Gordon, et al., *Astrophys. J.* **663**, 866 (2007).
7. O. V. Egorov, T. A. Lozinskaya, and A. V. Moiseev, *Mon. Not. R. Astron. Soc.* **429**, 1450 (2013).
8. C. W. Engelbracht, K. D. Gordon, G. H. Rieke, et al., *Astrophys. J.* **628**, 29 (2005).
9. H. L. Gomez, O. Krause, M. J. Barlow, B. M. Swinyard, et al., *Astrophys. J.* **760**, 96 (2012).
10. K. D. Gordon, Ch. W. Engelbracht, G. H. Rieke, et al., *Astrophys. J.* **682**, 336 (2008).
11. P. Hodge, N. V. Strobil, and R. C. Kennicutt, *Publ. Astron. Soc. Pacif.* **106**, 309 (1994).
12. L. K. Hunt, T. X. Thuan, Y. I. Izotov, and M. Sauvage, *Astrophys. J.* **712**, 164 (2010).
13. D. A. Hunter, F. C. Gillett, J. S. Gallagher, et al., *Astrophys. J.* **303**, 171 (1986).
14. R. C. Kennicutt, L. Armus, G. Bendo, D. Calzetti, et al., *Publ. Astron. Soc. Pacif.* **115**, 928 (2003).
15. R. C. Kennicutt, D. Calzetti, D. Aniano, et al., *Publ. Astron. Soc. Pacif.* **123**, 1347 (2011).
16. M. S. Khramtsova, D. S. Wiebe, P. A. Boley, and Ya. N. Pavlyuchenkov, *Mon. Not. R. Astron. Soc.* **431**, 2006 (2013).

17. C. Leitherer, D. Schaerer, J. D. Goldader, et al., *Astrophys. J.* **123**, 3 (1999).
18. A. K. Leroy, F. Walter, F. Bigiel, et al., *Astron. J.* **137**, 4670 (2009).
19. E. M. Levesque, L. J. Kewley, and K. L. Larson, *Astron. J.* **139**, 712 (2010).
20. M.-M. Mac Low and R. McCray, *Astrophys. J.* **324**, 776 (1988).
21. S. C. Madden, F. Galliano, A. P. Jones, and M. Sauvage, *Astron. Astrophys.* **446**, 877 (2006).
22. A. R. Marble, C. W. Engelbracht, L. van Zee, et al., *Astrophys. J.* **715**, 506 (2010).
23. J. S. Mathis, P. G. Mezger, and N. Panagia, *Astron. Astrophys.* **128**, 212 (1983).
24. J. Moustakas, R. C. Kennicutt, C. A. Tremonti, et al., *Astrophys. J. Suppl. Ser.* **190**, 233 (2010).
25. D. Puche, D. Westpfahl, E. Brinks, and J.-R. Roy, *Astron. J.* **103**, 1841 (1992).
26. K. M. Sandstrom, A. D. Bolatto, B. T. Draine, et al., *Astrophys. J.* **715**, 701 (2010).
27. D. Schaerer and W. D. Vacca, *Astrophys. J.* **497**, 618 (1998).
28. G. Stasińska and C. Leitherer, *Astrophys. J. Suppl. Ser.* **107**, 661 (1996).
29. S. G. Stewart, M. N. Fanelli, G. G. Byrd, et al., *Astrophys. J.* **529**, 201 (2000).
30. B. E. K. Sugerman, B. Ercolano, M. J. Barlow, et al., *Science* **313**, 196 (2006).
31. F. Walter, E. Brinks, W. J. G. de Blok, et al., *Astron. J.* **136**, 2563 (2008).
32. J. C. Weingartner and B. T. Draine, *Astrophys. J.* **548**, 296 (2001).
33. D. R. Weisz, E. D. Skillman, J. M. Cannon, et al., *Astrophys. J.* **689**, 160 (2008).
34. D. R. Weisz, E. D. Skillman, J. M. Cannon, et al., *Astrophys. J.* **704**, 1538 (2009).
35. D. S. Wiebe, O. V. Egorov, and T. A. Lozinskaya, *Astron. Rep.* **55**, 585 (2011).

Translated by V. Astakhov